International Journal of Mechanical, Industrial and Aerospace Sciences
ISSN: 2517-9950
Vol:14, No:3, 2020

The Effects of Electromagnetic Stirring on Microstructure and Properties of γ-TiAl Based Alloys Fabricated by Selective Laser Melting Technique

A. Ismaeel, C. S. Wang, D. S. Xu

Abstract—The γ-TiAl based Ti-Al-Mn-Nb alloys were fabricated by selective laser melting (SLM) on the TC4 substrate. The microstructures of the alloys were investigated in detail. The results reveal that the alloy without electromagnetic stirring (EMS) consists of γ-TiAl phase with tetragonal structure and α_2-Ti_3Al phase with hcp structure, while the alloy with applied EMS consists of γ-TiAl, α_2-Ti_3Al and α-Ti with hcp structure, and the morphological structure of the alloy without EMS which exhibits near lamellar structure and the alloy with EMS shows duplex structure, the alloy without EMS shows some microcracks and pores while they are not observed in the alloy without EMS. The microhardness and wear resistance values decrease with applied EMS.

Keywords—Selective laser melting, γ-TiAl based alloys, microstructure, properties, electromagnetic stirring.

I. Introduction

THe γ-TiAl based alloys are important candidate materials for high temperature applications, especially aerospace and automotive industries, due to their attractive properties such as low density, high specific strength and creep resistance [1]-[4]. However, the alloys suffer from low ductility and toughness at ambient temperature and are difficult to process by conventional processing routes [5], [6].

SLM is an additive manufacturing technique and enables the production of individual metal components with complex geometries layer by layer, according to a 3D-CAD volume model, without the need of part-specific tooling or preproduction costs [7]-[10], which provides a new approach for fabricating difficult-to-machine alloy components. In recent years, intensive researches have been performed in the SLM of γ-TiAl based alloys. the γ-TiAl based alloys fabricated by SLM, the microstructure of the alloys which exhibit extremely fine grains due to rapid solidification processing, leading to an improved the alloys property [11], [12].

The research of SLM of γ-TiAl based alloys confirmed that the microstructure of the alloys strongly depended on laser parameters, namely, the high laser energy density was leading to finer microstructure [9], [13]. In addition, the alloying elements are one of the most effective methods for the structural change and grain refinement. Therefore, the influences of various alloying elements in the fabrication of γ-TiAl based alloys were studied. The results showed that the microstructure significantly refined through the alloying with B, V, Y, Mo, and Cr elements [14]-[16]. However, the grain refinement is still limited. Due to high residual stresses associated with SLM during the solidification and the rapid solidification, this causes cracks and pores due to low ductility of γ-TiAl based alloys. With this respect, the EMS is applied, because the EMS can introduce a convective flow across the solid-liquid interface, on other hand, the introduction of a convective flow during solidification will redistribute the solute throughout the materials, thus, will increase the thermal expansion and reduce the residual stresses, temperature gradient, segregation, and lead to more grain refinement or structural changes. Therefore, in this work, the γ-TiAl based Ti-Al-Mn-Nb alloy without and with EMS is fabricated by SLM on the TC4 substrate. The effects of EMS on microstructure and properties of the alloy were investigated in detail and compared with the alloy without EMS.

A. Ismaeel is with the Institute of Metal Research, Chinese Academy of Sciences, Shenyang 110016, China, Key Laboratory of Materials Modification by Laser, Ion and Electron Beam, Dalian University of Technology, Dalian 116024, China.

C. S. Wang is with the Key Laboratory of Materials Modification by Laser, Ion and Electron Beam, Dalian University of Technology, Dalian 116024, China (corresponding author, phone: +86-411-84707930 e-mail: laser@dlut.edu.cn).

D. S. Xu is with the Institute of Metal Research, Chinese Academy of Sciences, Shenyang 110016, China.

II. Experimental Procedures

The pure Ti plate with the size of $30mm \times 20mm \times 20mm$ was chosen as a substrate material. The Al, Mn, and Nb for each element, 99.90 at% purity,-200mesh respectively, were blended by ball grinder according to the composition listed in Table I, which were chosen as SLM materials. There are four primary components of the SLM assembly: the laser system, the powder delivery system, the controlled environment, and the CAD is driven motion control system. A 5 KW continuous-wave CO_2 laser unit was used. Based on the preliminary experiments, the optimized laser processing parameters were adopted as follows: laser power 2.0 KW, laser beam diameter 3 mm, scanning velocity $2.5mm/s$, overlapping 30 at%, powder feed rate 3.0 g/min, the argon flow rate 7.0 L/min. Specimens with the size of $10mm \times 8mm \times 8mm$ were prepared using scanning strategies of cross-hatching.

During SLM processing, the laser beam was focused on the substrate to create a melt pool into which the powder feedstock is delivered through an inert gas (He) flowing through a special

TABLE I
CHEMICAL COMPOSITION OF TI-AL-MN-NB ALLOYS

Alloy	Composition(at.%)			
	Ti	Al	Mn	Nb
Without EMS	43	48	2	7
With EMS	43	48	2	7

nozzle, where the powder streams converge at the same point on the focused laser beam. An inert gas shroud containing argon was used as a protective atmospherefor preventing oxidation during deposition. And rotating EMS was applied with 80 mT.

Phase identification of these SLM samples was carried out using an XRD-6000 X-ray diffraction, equipped with a Ni filtered, Cu Ka radiation operating at 40 kV and 30 mA. The structural characteristics and composition were analyzed using a Zeiss Supra 55 (VP) scanning electron microscopy (SEM) and an EPMA-1720 electron probe micro-analyzer (EPMA). A DMH-2LS microhardness tester was used to measured microhardness under a load of 200 N with the duration of 15 s. And a Si3N4 ball with a diameter of 5.96 mm and a hardness of HV1500 were selected as the wear couple. The experiment was performed at a normal load of 10N, a sliding speed of 1.0 mm/s, and a wear time of 30 min.

III. RESULTS AND DISCUSSIONS

A. Microstructure

Fig. 1 shows the X-ray diffraction patterns of the alloys without and with EMS. The data reveal that the alloy without EMS mainly consists of γ-TiAl phase with tetragonal lattice and α_2-Ti_3Al phase with hcp structure as small volume fraction, while the alloy with EMS consists of γ-TiAl, α_2-Ti_3Al phase and α-Ti with hcp structure. Further quantitative analysis using reference intensity method reveals that the contents of the α_2-Ti_3Al phase increase with applied EMS, while those of the γ-TiAl phase change in the opposite trend. To investigate the effects of EMS on structural parameters, the lattice parameters of the constituent phases of the alloys without and with EMS are calculated using the least square method. As shown in Table II, the lattice parameters of γ-TiAl compound decrease with applied EMS, while those of the α_2-Ti_3Al compound show more increases in lattice parameters.

Fig. 2 presents the typical SEM morphologies of the alloys without and with EMS. As shown in Fig. 2 (a), there exist of inter-dendrites in the dark matrix, together with the bright phase in the alloy without EMS and the microstructure classified as near lamellar structure. EPMA analysis reveals that the inter-dendrite has a similar composition to the dark matrix, in which the atomic ratio of titanium and aluminum is nearly one to one, while the bright phase is rich in titanium as seen in Table III.

Combining with the XRD analysis, it is indexed that dendrite and dark matrix correspond to γ-TiAl phase, while the bright phase corresponds to α_2-Ti_3Al compound. In the alloy with applied EMS as shown in Fig. 2 (b), there exist

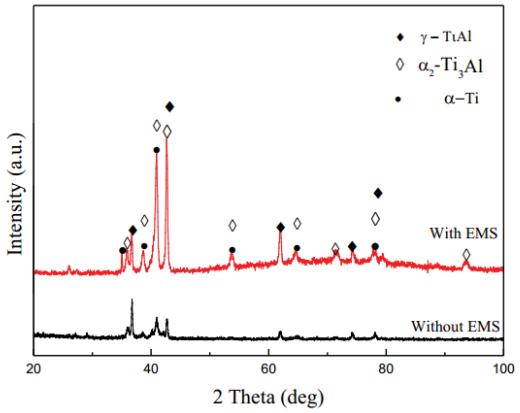

Fig. 1 X-ray diffraction patterns of the alloys without and with EMS

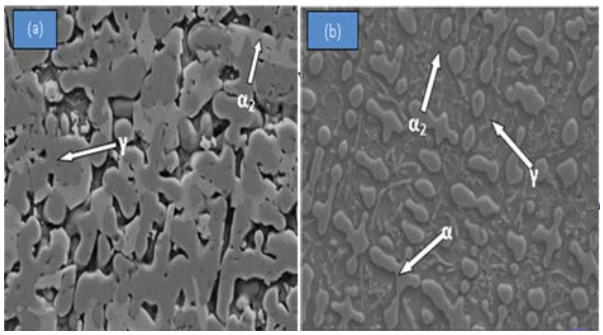

Fig. 2 SEM micrographs of the alloys (a) without EMS, (b) with EMS

equiaxed grain and lath-shaped in matrix, due to chemical elements distribution of the alloy obtained by EPMA shown in Fig. 3, the data revealed that the equiaxed grain corresponds to α-Ti phase, and lath-shaped to γ-TiAl compound, while the matrix corresponds to the α_2-Ti_3Al compound. Based on the above fact, it can be inferred that the microstructure evolution of the alloy without EMS during solidification process is as follows:

$L \longrightarrow \gamma \longrightarrow \gamma RL + \gamma \longrightarrow \gamma + \alpha_2$

The super-cooled liquid is solidified by the dendritic growth of the primary γ-TiAl phase followed by α-Ti transformation of the remaining interdendritic liquid (RL). Upon cooling, a eutectoid reaction of α-Ti occurs, leading to the formation of a mixture consisting of α_2-Ti_3Al plus γ-TiAl according to Ti-Al phase diagram Fig. 4, and exhibit near lamellar microstructure. While microstructure evaluation of the alloy with EMS during solidification process is as follows:

$\alpha + \gamma RL \longrightarrow \gamma + \alpha + \alpha_2$

TABLE II
THE LATTICE PARAMETERS OF THE CONSTITUENT PHASES

Alloy	γ-TiAl		α_2-Ti_3Al		α-Ti	
	a(nm)	c(nm)	a(nm)	c(nm)	a(nm)	c(nm)
Without EMS	0.4238	0.4279	0.3264	0.5328	—	—
With EMS	0.4152	0.4198	0.3328	0.5424	0.2137	0.3765

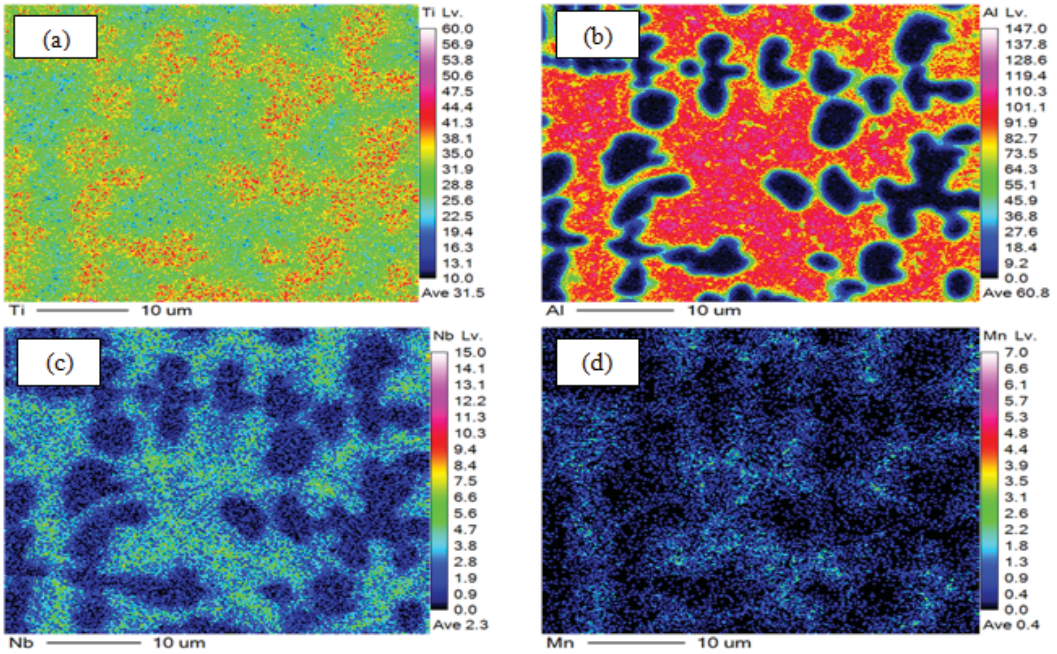

Fig. 3 EPMA chemical elements distribution of the alloy with EMS (a) Ti, (b) Al, (c) Nb and (d) Mn

The solidification pathway during the SLM processing of the alloy has been experienced a peritectic reaction which is solidified by the dendritic growth of the primary α-Ti phase, upon cooling followed by transformation of the remaining interdendritic liquid, leading to the formation of a mixture consisting of α-Ti, γ-TiAl and α_2-Ti_3Al phase according to Ti-Al phase diagram Fig. 4. The composition of the alloy gradually shifts towards rich-Ti zone, which not only decreases the volume fraction of the γ-TiAl phase, but also reduces the temperature range of solidification, with applied EMS, the introduction of a convective flow across the solid-liquid interface (SLI) and into the mushy zone during solidification of a metals, this process was redistributed the solute throughout the molten metals, thus, reduces the solute concentration gradient and temperature gradient in melt materials. The redistribution of the solute within the bulk liquid was leading to changes in segregation of the alloying leading to grain refinement. This in turn, enlarges primary dendrite spacing and increases the inter-dendritic fluid flow rate, causing the decreases of inter-dendritic segregation. As a result, the morphology of the γ-TiAl and α_2-Ti_3Al phase changes from near lamellar to lath-shaped in a matrix with applied EMS. The volume fraction of α_2-Ti_3Al phase is significantly increases due to the sequential shift of alloy composition towards rich-Ti zone, and microstructure is classified as a duplex structure. And the microcracks and pores are successfully reduced in compared with previous study.

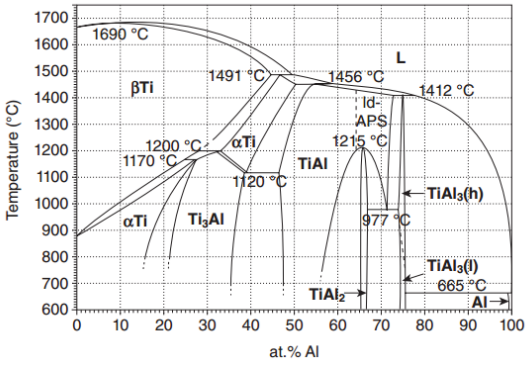

Fig. 4 Binary Ti Al phase diagram according to the assessment of Schuster and Palm [17]

IV. Microstructural Defects

A. microcracks

Fig. 5 shows the microcracks formed during the fabrication process, in fact, the rate of heat extraction is expected to decreases with each layer of the laser deposition due to a decrease in the temperature gradient between liquid and solid phase [18],[19]. Therefore, due to continuous heating, re-melting and high cooling rate, such instability by the variation at a temperature gradient of the laser deposition layers will lead to different grain size, small volume fraction and different thickness of the constituent phases, thus, leads to microcrack in fabricated alloys [20]. Furthermore, the microcrack formed near to substrate and directed toward the substrate due to the difference at a temperature gradient between the substrate and deposited layers, so the thermal instability becomes the main reason for microcrack formation. Despite the fact that the small molten pool in the existence of evaporated materials increases the stresses and reduces the thermal expansion of the molten materials and generated the

TABLE III
EPMA ANALYSIS RESULTS TAKEN FROM DIFFERENT AREAS OF THE ALLOY WITHOUT EMS

Alloy	Dendrite				Bright				Dark matrix			
	Ti	Al	Mn	Nb	Ti	Al	Mn	Nb	Ti	Al	Mn	Nb
Without EMS	44.2	48.5	1.6	5.7	60.7	36.1	1.7	1.5	46.5	46.7	1.5	5.3

cracks, because the bad interface between molten materials and substrate will increase the surface tension and formed the microcracks, as presented in the theory of SLM model [18], [21] and shown in Fig. 6.

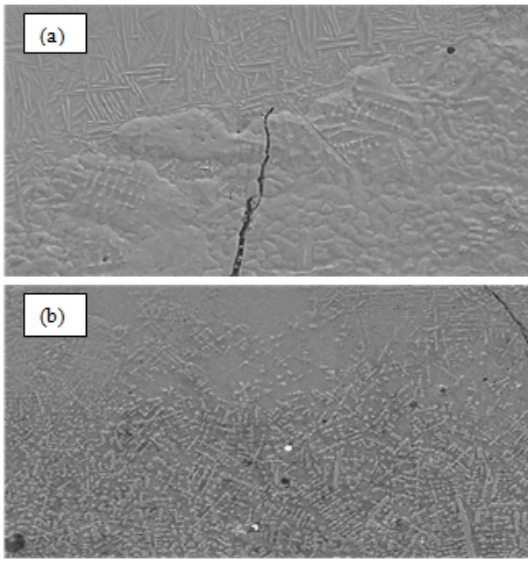

Fig. 5 Alloy without EMS Microcracks Mode

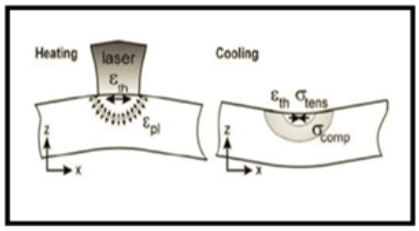

Fig. 6 SLM heating/Cooling diagram [18]

B. Pores

Fig. 7 shows the pores, the main reason for the pores formed during the laser fabricated materials due to very fast solidification, and some gases were involved in the materials The solidification rate is very high than the buoyancy velocity of the entrapped gasses in the melt materials and makes pores in the fabricated components [18], [20], [21]. On the other hand, if the energy input is not high enough to melt all the powders, it will lead to pores areas with partially molten or un-molten powders around it as shown in Figs. 7 (a) and (b). It can be assumed that contrary to the low energy input leading to pores in some regions because the energy input seems to be too high leading to thermal tensions which are not tolerated by the material and this results in thermal induced microcracks [18], [19]. This wormhole is generally caused when the intermediate cooling is present or might be due to an abnormal material flow during the welding. The porosity is an important factor in the final residual stress state, as the pores are stress-free zone in a highly stressed material, causing relaxation in the direct vicinity of the pores [18], [20]. Overall these microcracks and pores are also relatively correlated to the microhardness and ductility of the alloys increase and decrease with microhardness and this is in a good agreement with our previous work and confirmed by [18]-[21].

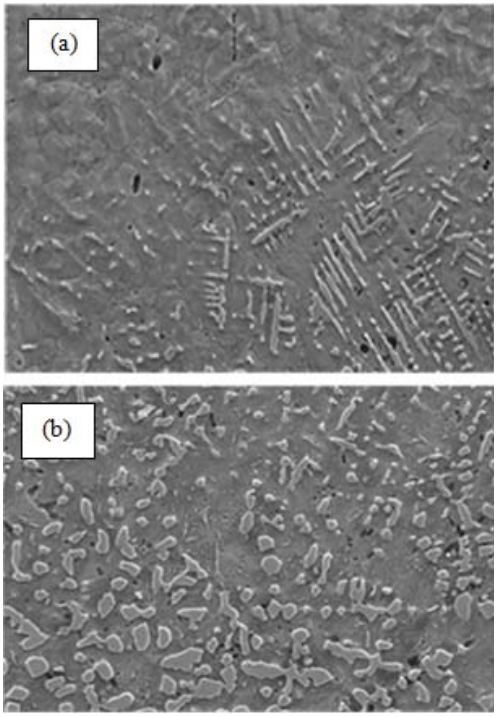

Fig. 7 Alloy without EMS pores Mode

V. PROPERTIES

A. Microhardness

The detailed investigation is on the average microhardness values of the alloys without and with EMS. For the alloy without EMS, high microhardness value is about 2000 Hv, while the microhardness value decreases with applied EMS and the value is about 1783 Hv. Despite the fact that the higher volume fraction of γ-TiAl for the alloy without EMS leads to the higher microhardness of the alloy, the higher

volume fraction of α-Ti and α_2-Ti_3Al decreases the volume fraction of γ-TiAl. The alloy with EMS plays a leading role in decreasing the microhardness of the alloy with applied EMS. In addition the EMS leading to more grain refinement meanwhile reduces solution strengthening of the alloy as the previous study and decreases the microhardness of the alloy.

B. Tribological Properties

The friction coefficient and worn volume of the alloy without and with EMS are 0.15, 0.08mm^3 and 0.22, 0.09mm^3 respectively, with the lowest friction coefficient and the lowest worn volume obtained by the alloy without EMS. In order to identify the mechanism underlying the above change values of the studied alloys, the worn surface morphologies of the alloys were observed by SEM shown in Fig. 8. The alloy without EMS owing to the formation of a near lamellar structure with high hardness and low lattice mismatch, only slight abrasive wear takes place on the worn surface of the alloy as shown in Fig. 8 (a). While for the alloy with applied EMS, the stress fatigue wear is obviously observed, because the formation of α-Ti, α_2-Ti_3Al and the fine lath-shaped γ-TiAl phase is quite effortlessly cut as shown in Fig. 8 (b). Despite the fact that higher volume fraction of α-Ti and α_2-Ti_3Al phase in the alloy reduced the anti-abrasive wear ability due to a decrease of microhardness, which is demonstrated by broader and deeper plowing grooves. The schematic diagram of rotating EMS flow pattern shown in Fig. 9.

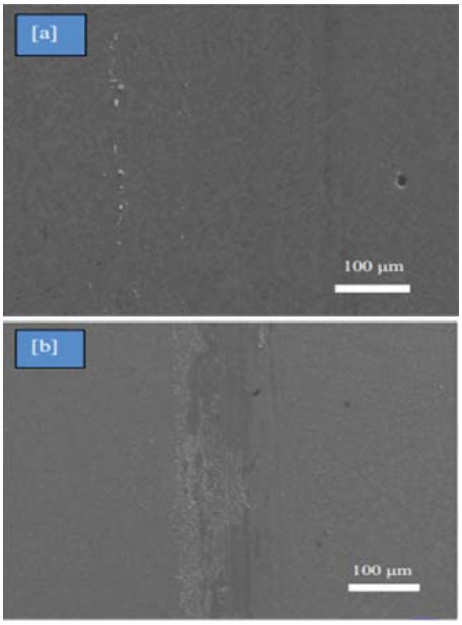

Fig. 8 Worn surface of the alloys (a) without EMS and (b) with EMS

VI. Conclusion

The EMS is very effective to structural changes and grain refinement. The microcracks and pores associated with high residual stress of SLM, rapid solidification and low ductility of γ-TiAl based alloys are completely reduced with applied EMS. Meanwhile the microhardness and tribological properties decrease with applied EMS, due to reduction in the volume fraction of γ-TiAl and increases of α_2-Ti_3Al and α-Ti, we strongly recommend more research of SLM with applied EMS.

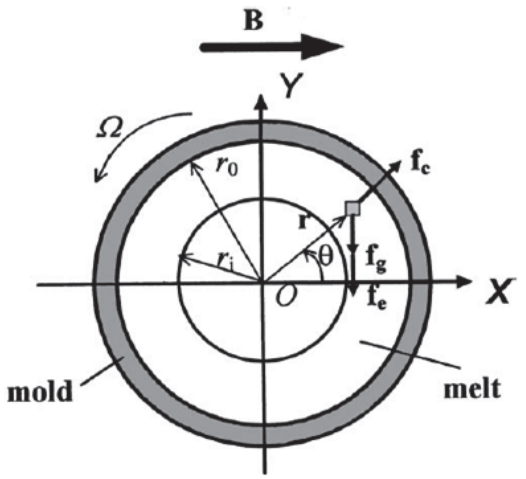

Fig. 9 Flow pattern generated by rotational EM field [22]

Acknowledgment

This study was supported by (CSC) Chinese scholarship council and the National Natural Science Foundation of China (No. 51371041).

References

[1] D. Srivastava, *Microstructural characterization of the γ-TiAl alloy samples fabricated by direct laser fabrication rapid prototype technique*. Bulletin of Materials Science, 2002, p. 619-633.
[2] D. Srivastava,I. Chang, and M. Loretto *The effect of process parameters and heat treatment on the microstructure of direct laser fabricated TiAl alloy samples*. Intermetallics, 2001, p. 1003-1013.
[3] D. Srivastava, et al. *The influence of thermal processing route on the microstructure of some TiAl-based alloys*. Intermetallics, 1999, p. 1107-1112.
[4] H.P. Qu, et al. *The effects of heat treatment on the microstructure and mechanical property of laser melting deposition γ-TiAl intermetallic alloys*. Materials and Design, 2010, p. 2201-2210.
[5] A. Menand, H. Zapolsky-Tatarenko,and A. Nrac-Partaix. *Atom-probe investigations of TiAl alloys*. Materials Science and Engineering A, 1998, p. 55-64.
[6] S.Z. Zhang, et al. *Microstructure and tensile properties of hot fogred high Nb containing TiAl based alloy with initial near lamellar microstructure*. Materials Science and Engineering A, 2015, p. 16-21.
[7] C. Kenel, et al. *MSelective laser melting of an oxide dispersion strengthened (ODS) γ-TiAl alloy towards production of complex structures*. Materials and Design, 2017.
[8] X.P. Li, J.V. Humbeeck, and J.P. Kruth. *Selective laser melting of weak-textured commercially pure titanium with high strength and ductility: A study from laser power perspective*. Materials and Design, 2017, p. 352-358.
[9] W. Li, et al. *SEffect of laser scanning speed on a Ti-45Al-2Cr-5Nb alloy processed by selective laser melting: Microstructure, phase and mechanical properties*. Journal of Alloys and Compounds, 2016, p. 626-636.
[10] G. Yang, et al. *Microstructures of as-Fabricated and Post Heat Treated Ti-47Al-2Nb-2Cr Alloy Produced by Selective Electron Beam Melting(SEBM)*. Rare Metal Materials and Engineering, 2016.

[11] M. Thomas, et al. *The prospects for additive manufacturing of bulk TiAl alloy*. High Temperature Technology, 2016, p. 571-577.
[12] J. Gussone, et al. *Microstructure of γ-titanium aluminide processed by selective laser melting at elevated temperatures*. Intermetallics, 2015, p. 133-140.
[13] L. Lober, et al. *Selective laser melting of a beta-solidifying TNM-B1 titanium aluminide alloy*. Journal of Materials Processing Technology, 2014, p. 1852-1860.
[14] Y.Z. Zhao, et al. *Microstructural evolution of hot-forged high Nb containing TiAl alloy during high temperature tension*. Materials Science and Engineering ,2016,p.116-121.
[15] E.T. Zhao, et al. *Microstructural control and mechanical properties of a β-solidified γ-TiAl alloy Ti-46Al-2Nb-1.5V-1Mo-Y*. Materials Science and sengineering:A, 2017, p. 1-6.
[16] H. Jabbar, et al. *Microstructures and deformation mechanisms of a G4 TiAl alloy produced by spark plasma sintering*. Acta Materialia, 2011, p. 7574-7585.
[17] F. Appel, J.D.H. Paul, and M. Oehring. *Gamma Titanium Aluminide Alloys (Science and Technology) Applications, Component Assessment, and Outlook*. Wiley-VCH Verlag GmbH and Co. KGaA, 2010.
[18] M.F. Zaeh, and G. Branner. *Investigations on residual stresses and deformations in selective laser melting*. Production Engineering.2010, P. 35-45.
[19] B. Vrancken, et al. *Residual stress via the contour method in compact tension specimens produced via selective laser melting*. Scripta Materialia. 87, p. 29-32.
[20] B. L. Van Belle, G. Vansteenkiste, and J.C. Boyer. *Investigation of residual stresses induced during the selective laser melting process*. Trans Tech Publ. 2013.
[21] P. Mercelis and J.P. Kruth. *Residual stresses in selective laser sintering and selective laser melting*. Rapid prototyping journal. 2006, P. 254-265.
[22] J. H Matthew,et al. *Effect of electromagnetic stirring on grain refinement of Al-(4.5%)Cu alloy*. Thesis submitted to the University of Alabama. 2013.